

Generic Strategy of Preparing Fluorescent Conjugated-Polymer-Loaded Poly(DL-lactide-co-Glycolide) Nanoparticles for Targeted Cell Imaging

By Kai Li, Jie Pan, Si-Shen Feng, Arthur Wenqing Wu, Kan-Yi Pu, Yutao Liu, and Bin Liu*

A general strategy for the preparation of highly fluorescent poly(DL-lactide-co-glycolide) (PLGA) nanoparticles (NPs) loaded with conjugated polymers (CPs) is reported. The process involves encapsulation of organic-soluble CPs with PLGA using a modified solvent extraction/evaporation technique. The obtained NPs are stable in aqueous media with biocompatible and functionalizable surfaces. In addition, fluorescent properties of the CP-loaded PLGA NPs (CPL NPs) could be fine-tuned by loading different types of CPs into the PLGA matrix. Four types of CPL NPs are prepared with a volume-average hydrodynamic diameter ranging from 243 to 272 nm. The application of CPL NPs for bio-imaging is demonstrated through incubation with MCF-7 breast cancer cells. Confocal laser scanning microscopy studies reveal that the CPL NPs are internalized in cytoplasm around the nuclei with intense fluorescence. After conjugation with folic acid, cellular uptake of the surface-functionalized CPL NPs is greatly enhanced via receptor-mediated endocytosis by MCF-7 breast cancer cells, as compared to that for NIH/3T3 fibroblast cells, which indicates a selective targeting effect of the folate-functionalized CPL NPs in cellular imaging. The merits of CPL NPs, such as low cytotoxicity, high fluorescence, good photostability, and feasible surface functionalization, will inspire extensive study of CPL NPs as a new generation of probes for specific biological imaging and detection.

which possess unique functional and structural properties not observed in discrete molecules or bulk materials, have been widely used in molecular imaging, cellular imaging, and medical diagnostics.^[4] As for cellular imaging, great interest has been focused on colloidal inorganic semiconductor quantum dots (QDs).^[5] QDs have shown narrow emission and high brightness and can be easily functionalized through surface modification.^[6] However, the concentration-dependent cytotoxicity of QDs, mainly caused by oxidative degradation of the heavy metal components, remains a problem although various modifications have been made to coat QD cores with a ZnS shell or further encapsulate QDs with biocompatible polymeric matrixes.^[7] The growing interest and booming development in biological detection motivated us to explore novel fluorescent probes with the hope of overcoming the limitations in stability and cytotoxicity to satisfy highly sensitive assays.

Conjugated polymers (CPs) are macromolecules with π -conjugated backbones, which allow the formation of excitons to facilitate photo- and electroluminescence. Various CPs have been reported to show high extinction coefficient and high fluorescence.^[8] Due to their highly delocalized backbone structures and unique electronic and optical properties, CPs have been widely used for electronics and biosensor applications.^[9] Recently, the application of CPs for cellular imaging has also been reported.^[10] The main obstacle in the application of CPs for biosensors or cellular imaging is their insufficient water solubility. One strategy is to introduce hydrophilic or ionic functional groups to CPs. The synthetic procedures generally require many steps, which are time-consuming. As compared to the sophisticated modification of polymer structures, an easier way is to prepare CP-based NPs. By precisely controlling the experimental conditions, CP NPs with different sizes can be prepared through the nanoprecipitation method, which show high fluorescence and limited blinking.^[11] However, further encapsulation is necessary to provide these CP NPs with functional surfaces for bioconjugation and specific target detection.

1. Introduction

Cellular imaging using fluorescent probes is an important technique in understanding the function and mechanism of target biological species in cells.^[1] Fluorescent proteins^[2] and organic dyes^[3] are widely used to label cells and subcellular targets due to their small size and good biocompatibility. However, poor photostability limits their applicability and sensitivity, especially in long-term studies. Recently, fluorescent nanoparticles (NPs),

[*] Prof. B. Liu, K. Li, J. Pan, Prof. S.-S. Feng, A. W. Wu, K.-Y. Pu, Y. T. Liu
Department of Chemical and Biomolecular Engineering
National University of Singapore
Singapore 117576 (Singapore)
E-mail: cheliub@nus.edu.sg

DOI: 10.1002/adfm.200901098

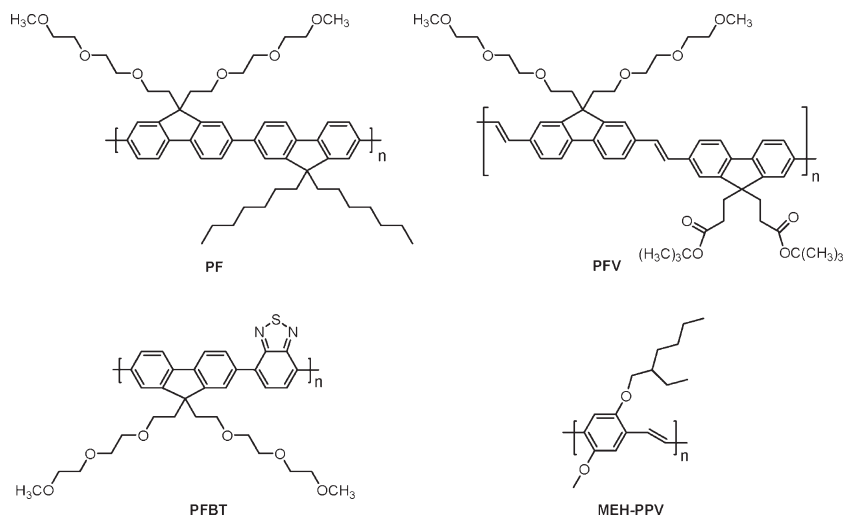
In this contribution, we report a simple strategy which allows the formation of biocompatible and surface-functionalizable CP-based NPs in one step using poly(DL-lactide-co-glycolide) (PLGA) as a matrix polymer. PLGA is one of the most widely used biocompatible polymers for preparing polymeric NPs in drug delivery system, which is reported to benefit the NP–cell interaction and enhance the cellular uptake efficiency.^[12] Formation of CP-loaded PLGA NPs (CPL NPs) is conducted through a modified solvent extraction/evaporation single-emulsion method with poly(vinyl alcohol) (PVA) as emulsifier.^[12] The excess terminal –COOH groups of PLGA exposed to water allow further functionalization of the CPL NPs. The synthesis of CPL NPs and their application in cellular imaging are studied, and the use of folic-acid-functionalized CPL NPs for targeted cell imaging is demonstrated. Because many neutral CPs with known optical properties have been reported in the literature, this strategy provides a general approach for preparing highly fluorescent and surface-amendable NPs with desired optical properties.

2. Results and Discussion

2.1. Characterization of CPL NPs

To demonstrate the generality of this strategy in preparing CPL NPs, four polymers with different fluorescent colors were selected; these include poly[9,9-dihexylfluorene-*alt*-9,9-bis(2-(2-methoxyethoxy)ethoxy)ethyl]fluorene] (PF), poly[9,9-bis(2-(2-methoxyethoxy)ethoxy)ethyl]fluorenyldivinylene-*alt*-9,9-bis(3-*t*-butylpropanoate)fluorene] (PFV), poly[9,9-bis(2-(2-methoxyethoxy)ethoxy)ethyl]fluorene-*alt*-4,7-(2,1,3-benzothiazol)] (PFBT), and poly[2-methoxy-5-(2'-ethyl-hexyloxy)-1,4-phenylene vinylene] (MEH-PPV). The chemical structures of the polymers are shown in Scheme 1.

Figure 1 shows the fluorescence spectra and the corresponding fluorescent color of the as-prepared CPL NP aqueous suspensions. The emission maxima for PF-, PFV-, PFBT-, and MEH-PPV-loaded NP suspension are 422, 481, 552, and 595 nm, respectively,



Scheme 1. Chemical structures of PF, PFV, PFBT, and MEH-PPV.

which corresponds to blue, green, yellow, and red fluorescence. As compared to the fluorescence spectra of corresponding CP solutions in dichloromethane (DCM) (Fig. S1a, Supporting Information (SI)), the maximum emission peaks of PF-, PFV-, PFBT-, and MEH-PPV-loaded NP suspension are red-shifted by 9, 2, 3, and 37 nm, respectively. A similar red-shift is also observed when one compares the emission maximum of each CP film and that of the corresponding CP solution in DCM (Fig. S1b, SI). The red-shift of the maximum emission peaks for these NPs is mainly caused by aggregation of CP molecules upon NP formation, which increases the interactions between segments of the polymer chains^[13] and favors energy transfer to low-energy defects and weakly fluorescent aggregates.^[14] A similar red-shift is observed for CP NPs prepared through nanoprecipitation.^[14] These results indicate that the optical properties of CPL NPs are mainly determined by the CP molecules loaded in the NPs, suggesting that CPL NPs with various colors and unique optical properties can be achieved by utilizing specific CPs.

Table 1 shows that the CPL NPs have a volume-average hydrodynamic diameter ranging from 243 to 272 nm, determined by the laser light scattering (LLS). PLGA-encapsulated NPs with a similar size have been proven efficient for cellular uptake.^[12] The zeta potential of CPL NPs is measured to be larger than –30 mV. The value of zeta potential reflects the effective charge on the particle surface and is therefore related to the electrostatic repulsion among particles. The negative value of zeta potential for CPL NP suspensions is due to the –COOH groups on the particle surface,^[15] which provide good colloidal stability for the NP suspensions. The CP encapsulation efficiency for these four types of CPL NPs is $\approx 45\%$ by comparing the fluorescence intensity of the freeze-dried NPs dissolved in DCM to that of a calibration curve. The stability of the CPL NPs is also studied by monitoring the amount of CP molecules released from the CPL NPs suspended in phosphate buffered saline (PBS) at 37 °C. The amount of released CP molecules is obtained by centrifugation of the NP suspension and extraction of the supernatant with DCM to monitor the fluorescence intensity. As shown in Table 1, the very low percentage of released CP molecules indicates excellent stability of the CPL NPs as compared to that of small-molecule dye-loaded (coumarin-6) PLGA NPs, which showed $\approx 0.32\%$ leakage in 24 h.^[16] The high stability can be attributed to the entanglement among the polymer chains of PLGA and CP, which blocks the diffusion of CP molecules into the aqueous phase. The extremely low release of CP molecules guarantees reliable results obtained in cellular imaging and cellular uptake experiments.

The field-emission scanning electron microscopy (FESEM) and transmission electron microscopy (TEM) images of PFV-loaded NPs are shown in Figure 2, while the images for the other three types of NPs are shown in Figure S2 and S3 (SI). The FESEM images reveal that the CPL NPs are spherical in shape with smooth surfaces, and the NPs prepared from different CPs show similar surface morphology. In the TEM images, the black dots indicate that the CP molecules are entangled and encapsulated in

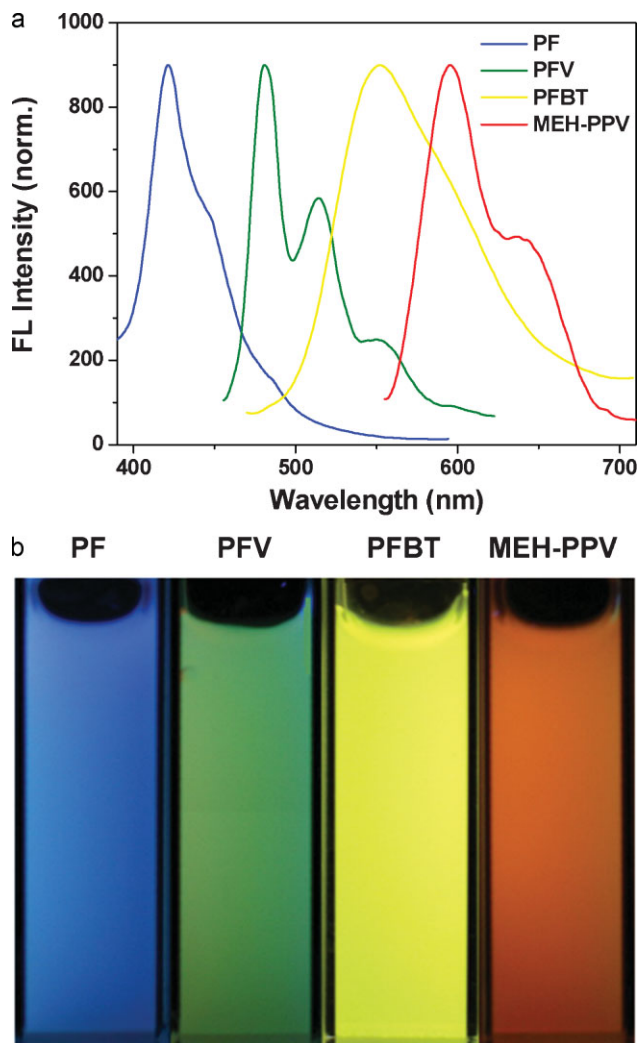


Figure 1. a) Fluorescence spectra of the CPL NP aqueous suspensions (excitation wavelength, $\lambda_{\text{ex}} = 370$ nm for PF, $\lambda_{\text{ex}} = 407$ nm for PFV, $\lambda_{\text{ex}} = 458$ nm for PFBT, and $\lambda_{\text{ex}} = 488$ nm for MEH-PPV). b) A photograph of NP aqueous suspensions captured by digital camera under a hand-held UV lamp.

the PLGA matrix. The particle size observed from FESEM and TEM images is smaller than that determined by LLS, which is mainly caused by the shrinkage of the polymeric NPs during the sample preparation in vacuum. A similar phenomenon has also

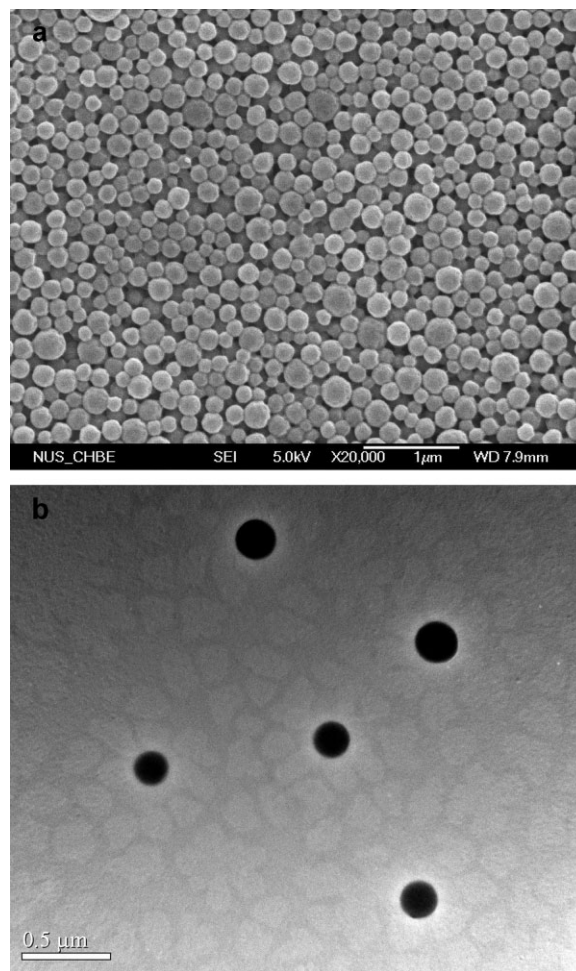


Figure 2. a) FESEM and b) TEM images of the PFV-loaded PLGA NPs with PVA as emulsifier.

been observed for other polymeric NPs.^[17] These results suggest that the solvent extraction/evaporation single-emulsion method using PLGA as an encapsulation matrix is a general strategy for the preparation of various types of CPL NPs with similar morphology. As compared to the irregular morphology of pure PFV NPs prepared under the same conditions in the absence of PLGA (Fig. S4, SI), the results shown in Figure 2, S2, and S3 (SI) indicate that the PLGA polymer matrix is essential for the formation of high-quality CPL NPs under our experimental conditions.

Table 1. Characteristics of the CPL NPs.

| Loaded CP | PF | PFV [b] | PFBT | MEH-PPV |
|------------------------------|---------------|---------------|---------------|---------------|
| Particle size [nm] [a] | 261.2 ± 4.5 | 257.5 ± 4.2 | 242.9 ± 3.8 | 271.4 ± 5.2 |
| Polydispersity [a] | 0.129 ± 0.034 | 0.124 ± 0.031 | 0.120 ± 0.028 | 0.158 ± 0.037 |
| Zeta potential [mV] | −36.61 | −37.15 | −33.42 | −35.28 |
| Encapsulation efficiency [%] | ≈41.3 | ≈43.9 | ≈44.2 | ≈47.6 |
| Leakage of CP in 5 days [%] | 0.095 | 0.098 | 0.087 | 0.062 |

[a] The particle size and polydispersity of NPs are determined by LLS. [b] For pure PFV NPs prepared without PLGA, the particle size is 221 ± 7.3 nm, and the polydispersity is 0.186 ± 0.049 .

2.2. Application of CPL NPs in Cellular Imaging

The application of the as-prepared CPL NPs in cellular imaging was studied by confocal laser scanning microscopy (CLSM). In these experiments, MCF-7 breast cancer cells were individually incubated in culture medium with different NP suspensions for 2.5 h at a CP concentration of 87.5 nM (based on polymer chain). The calculation of CP concentration and its correlation with NP concentration is described in the SI. The CLSM images of MCF-7 cancer cells after incubation with PFV-loaded NP suspension are shown in Figure 3. These images were taken upon excitation at 405 nm (5% laser power) with a band pass 465–495 nm filter. The images of MCF-7 cancer cells after incubation with the other three types of CPL NPs are shown in Figure S5 (SI). In Figure 3, the fluorescence image (C) is the overlaying image of (A) and (B). Obvious green fluorescence is observed in the cytoplasm around the nuclei (red, stained by propidium iodide), indicating that the PFV-loaded NPs are internalized by the cells. The pure PFV NPs without the PLGA matrix is also used as a control to evaluate the effect of PLGA on cellular uptake. When the same amount of MCF-7 cancer cells is incubated with the pure PFV NPs at 87.5 nM PFV, there is only a very weak PFV fluorescent signal observed. Quantitative cellular uptake of NPs by MCF-7 cancer cells was also studied for the PFV-loaded NPs and pure PFV NPs at 87.5 nM PFV. After incubation for 2.5 h, the cellular uptake efficiency of PFV-loaded NPs is $\approx 31\%$, which is much higher than that of pure PFV NPs ($\approx 8.5\%$), indicating that the PLGA matrix can sufficiently elevate the MCF-7 cellular uptake of NPs.

2.3. Cytotoxicity of CPL NPs

The cytotoxicity of the CPL NPs was evaluated by metabolic viability of NIH/3T3 fibroblast cells after incubation with the CPL

NPs. Figure 4a shows the cell viability after incubation with PFV-loaded NP suspension at PFV concentrations of 700, 350, and 87.5 nM for 12, 24, and 48 h, respectively. The metabolic viability of NIH/3T3 cells does not change after incubation with PFV-loaded NP suspension even at 700 nM PFV, indicating the low cytotoxicity of PFV-loaded NPs. Similar results were also obtained for the other three types of CPL NPs, which indicated the low cytotoxicity of CPL NPs to NIH/3T3 fibroblast cells within the tested period (Fig. S6, SI). Furthermore, unlike the concentration-dependent cytotoxicity of QDs reported in the literature,^[7a,c] the cytotoxicity of CPL NPs is independent of NP concentrations, which ensures their applications in real practice at high concentrations when necessary. The metabolic viability of NIH/3T3 cells after incubation with the pure PFV NPs without a PLGA matrix also did not show any obvious decrease under the same experimental conditions. This result further confirms that the CPL NPs are of low toxicity to the cells, which is superior to QDs.

2.4. Targeted Cancer Cell Imaging

The mechanism of cellular uptake for NPs can be affected by various factors, including the particle size, charge, and surface chemistry.^[18] One efficient method to improve cellular uptake and specific targeting effect of the NPs is to modify their surfaces with ligands which have specific interaction with the receptors over-expressed in the cell membrane. Folic acid has been widely used as a ligand to modify NPs to achieve cell-specific internalization via receptor-mediated endocytosis for drug delivery and cellular imaging.^[19] It takes advantage of the high binding affinity ($K_d \approx 100$ pM) between folic acid and folate receptors which have a low expression level in normal cells,^[20] but are over-expressed in several kinds of cancer cells, such as breast, ovarian, kidney, and prostate cancer cells. As a consequence, targeted MCF-7 breast cancer cell imaging can be realized using folic acid-functionalized CPL NPs, due to the much higher folate receptor expression level in the breast cancer cell membrane compared to that of NIH/3T3 fibroblast cells.^[21]

The functionalization of PFV-loaded NPs was carried out through a *N*-(3-dimethylaminopropyl)-*N'*-ethylcarbodiimide hydrochloride (EDAC)-mediated coupling reaction between the –COOH groups of the PLGA matrix and the amino groups of aminated folic acid, as illustrated in Scheme 2. The amination of folic acid was carried out according to literature.^[22] After functionalization, the zeta potential of PFV-loaded NP aqueous suspension decreased from -37.15 to -22.3 mV, which is due to the reduced carboxyl groups on the NP surface after conjugation with aminated folic acid. The presence of folic acid on the NP surface is further confirmed by X-ray photoelectron spectroscopy (XPS), which provides the chemical composition of the particle surface (Fig. S7, SI). As there is no elemental nitrogen in the pristine PFV-loaded NPs, the peak at 397.6 eV in the spectrum of folate-functionalized

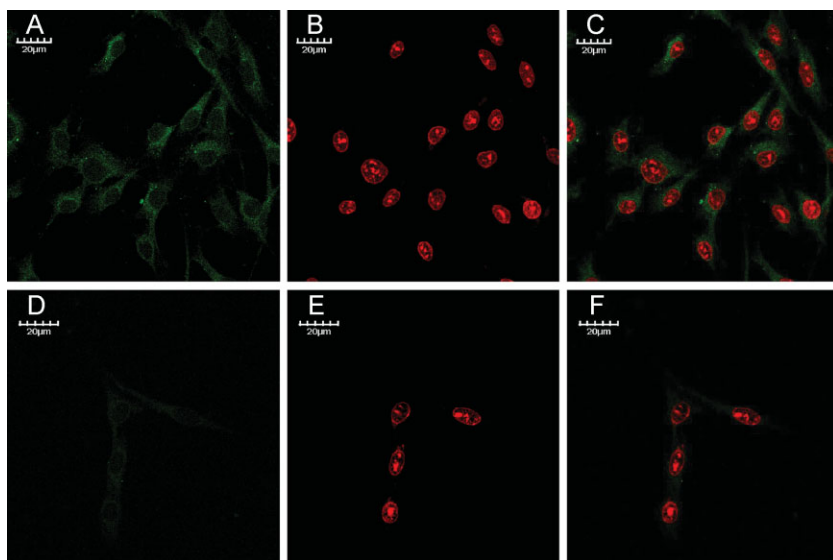


Figure 3. CLSM images of the MCF-7 breast cancer cells after 2.5 h incubation with the PFV-loaded PLGA NP suspension (A, B, and C) and pure PFV NP suspension (D, E, and F) at 87.5 nM PFV. The detection of PFV fluorescence is achieved by excitation at 405 nm (5% laser power) with a band pass 465–495 nm filter. Overlaying images in the right column are obtained from the combination of the left and middle column.

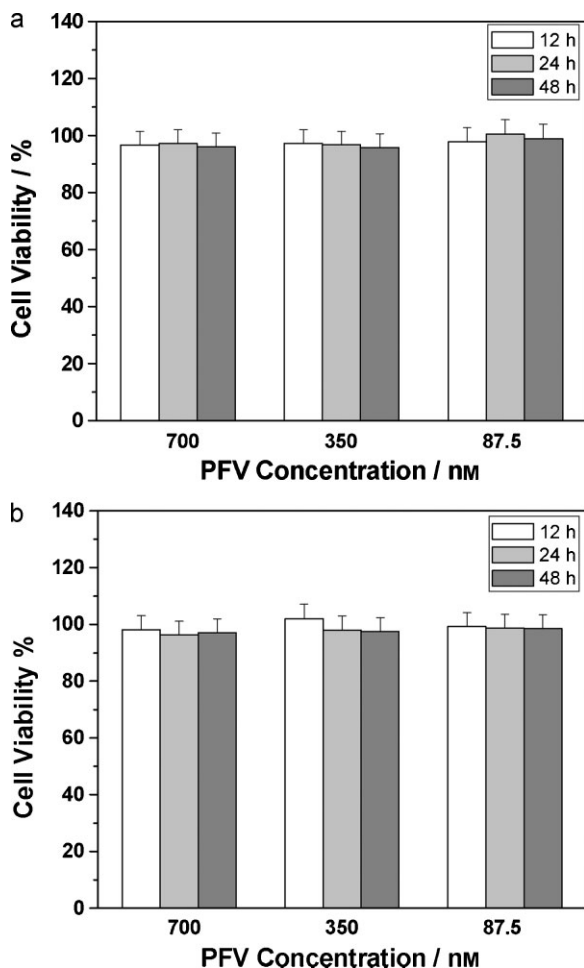
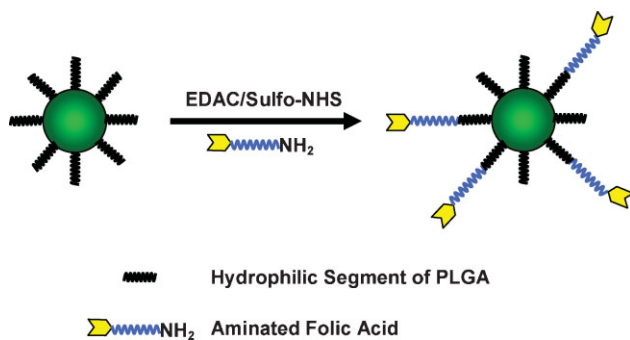


Figure 4. Metabolic viability of NIH/3T3 fibroblast cells after incubation with the PFV-loaded PLGA NP suspension (a) and pure PFV NP suspension (b) at different PFV concentrations for 12, 24, and 48 h, respectively.



Scheme 2. Schematic representation of folic acid functionalization of the PFV-loaded PLGA NPs.

(FA) PFV-loaded NPs indicates the presence of folic acid on the NP surface after conjugation. The conjugation efficiency of aminated folic acid to $-\text{COOH}$ on NPs is $\approx 24\%$ (see SI).

Figure 5A shows the CLSM image of the MCF-7 breast cancer cells after incubation for 2.5 h with the FA PFV-loaded NP suspension in culture medium at 87.5 nM PFV. The bright green fluorescence from NPs in the cells remains clearly distinguishable

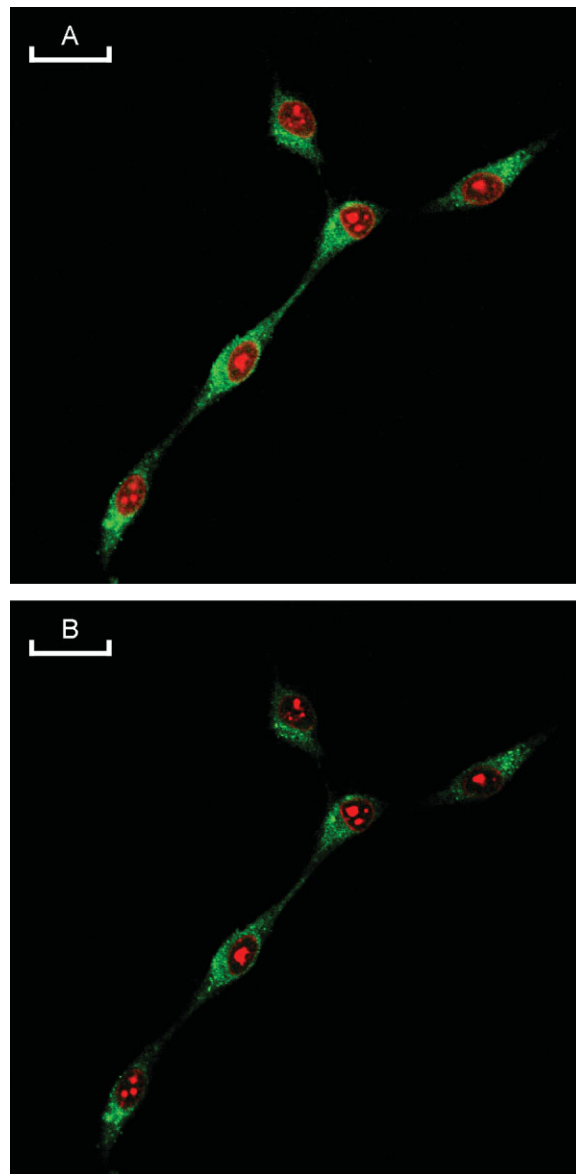


Figure 5. CLSM images of the MCF-7 breast cancer cells after 2.5 h incubation with the FA PFV-loaded PLGA NP suspension at 87.5 nM PFV. The images are obtained after continuous excitation at 405 nm (5% laser power) for 0 (A) and 20 min (B) with a band pass 465–495 nm filter.

after continuous laser excitation at 405 nm for 20 min (Fig. 5B), indicating good stability of PFV-loaded NPs. Under the same experimental conditions, much higher fluorescence intensity is shown in Figure 5A as compared to that in Figure 3C. Considering that the slight variation in surface zeta potential does not obviously affect the cellular uptake of PFV-loaded NPs by MCF-7 breast cancer cells (Fig. S8, SI), these results indicate that more FA PFV-loaded NPs are internalized by MCF-7 cells via receptor-mediated endocytosis. Quantitative studies reveal that the cellular uptake efficiencies for FA PFV-loaded NPs and PFV-loaded NPs are 47% and 31%, respectively. Moreover, the 3D CLSM image was obtained, showing that the green fluorescence is mainly from the

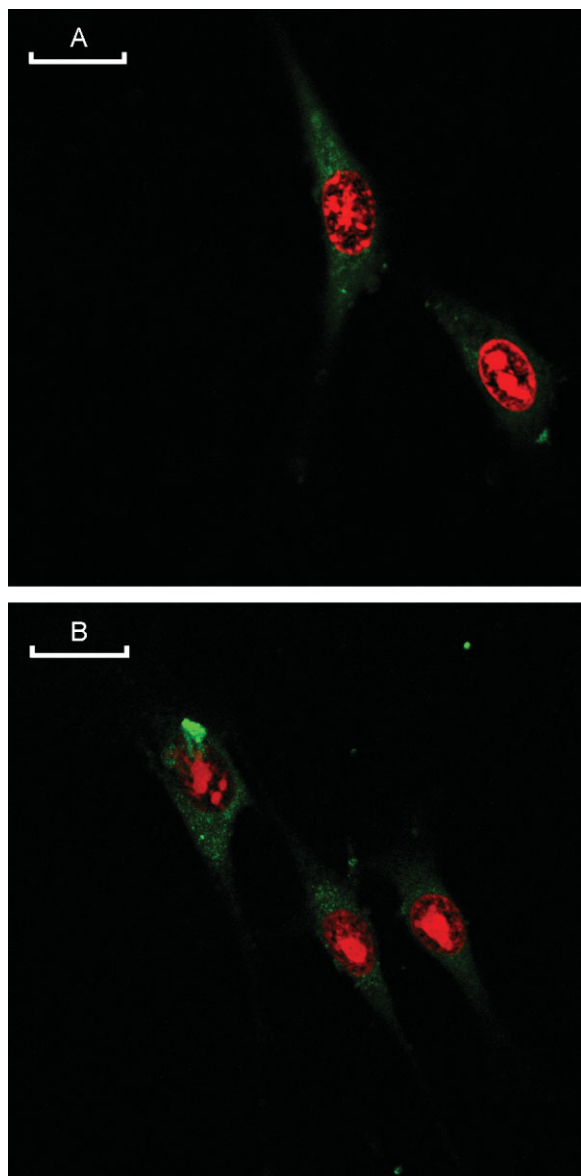


Figure 6. CLSM images of the NIH/3T3 fibroblast cells after 2.5 h incubation with the PFV-loaded PLGA NP suspension (A) and FA PFV-loaded PLGA NP suspension (B) in culture medium at 87.5 nM PFV. The images are obtained after continuous excitation at 405 nm (5% laser power) with a band pass 465–495 nm filter.

FA PFV-loaded NPs internalized in the cell cytoplasm rather than from those on the cell surface (Fig. S9, SI). In addition, PFV-loaded NPs treated with free aminated folic acid in the absence of EDAC and *N*-hydroxysulfosuccinimide sodium salt (Sulfo-NHS) were also used as a control for cellular uptake studies of MCF-7 cancer cells. The CLSM image (Fig. S10, SI) reveals that the green fluorescence intensity is similar to that for PFV-loaded NPs shown in Figure 3C. These results suggest that the targeting effect of the FA PFV-loaded NPs is due to the conjugation of folic acid onto the NP surface rather than the nonspecific interaction between free folic acid and NPs.

As a low-folate-receptor control group, NIH/3T3 fibroblast cells were incubated with the suspensions of PFV-loaded NPs and FA PFV-loaded NPs for 2.5 h at 87.5 nM PFV, respectively. Figure 6 shows the CLSM images of the NIH/3T3 cells after incubation. There is no obvious difference in green fluorescence intensity for NIH/3T3 cells upon incubation with both NPs, mainly due to the low expression level of the folate receptor in NIH/3T3 cell membrane, which does not significantly favor internalization of the FA PFV-loaded NPs. Meanwhile, comparison between Figure 6B and 5A indicates that the cellular uptake of FA PFV-loaded NPs by NIH/3T3 fibroblast cells is much lower than that by MCF-7 cancer cells. These results suggest that the folic acid functionalization renders the NPs targeting effect to cancer cells with an over-expression of folate receptors in the membrane. Based on this understanding, the surface-functionalized CPL NPs can provide helpful information in early cancer detection.

3. Conclusion

We report a general method to fabricate CP-loaded PLGA NPs through a solvent extraction/evaporation single-emulsion method. The CP-loaded PLGA NPs are of low cytotoxicity with high brightness and good photostability. Upon incubation of CPL NPs with MCF-7 breast cancer cells, bright fluorescence was observed in the cytoplasm around the nuclei. The PLGA matrix also allows further modification of the NP surface with ligands for specific recognition of biological targets. Using PFV-loaded NPs as an example, after functionalization of the PFV NPs with folic acid, the uptake of FA PFV NPs by MCF-7 cells was improved via receptor-mediated endocytosis. Furthermore, the folate-functionalized NPs showed specific targeted imaging for MCF-7 breast cancer cells that had over-expressed folate receptors in the membrane. Since this strategy provides a universal concept for preparing CP-loaded NPs using hydrophobic CPs, multicolor and multifunctional CP-loaded NPs with brighter fluorescence and better photostability could be achieved to satisfy the growing demands in biological application with the development of conjugated polymers. However, this PLGA-based NP formation is not suitable for providing small NPs similar to those prepared by nanoprecipitation. Further optimization of this one-step strategy using different matrix polymers is likely to yield CPL NPs with desirable particle sizes that could meet the requirements for various biological applications.

4. Experimental

Materials: PF ($M_w = 30\,000$, PDI = 2.3), PFV ($M_w = 83\,000$, PDI = 2.3), and PFBT ($M_w = 36\,000$, PDI = 2.8) were synthesized according to the literature [23]. MEH-PPV ($M_w > 50\,000$) was purchased from American Dye Source, Inc. PLGA (L:G molar ratio: 50:50, M_w : 100 000–130 000) was a gift from PURAC Asia Pacific, Singapore. PVA (M_w : 30 000–70 000), EDAC, *N*-hydroxysuccinimide (NHS), Sulfo-NHS, MTT, penicillin–streptomycin solution, trypsin–EDTA solution, and *N,N'*-dicyclohexylcarbodiimide (DCC) were purchased from Sigma–Aldrich. Fetal bovine serum (FBS) was purchased from Gibco (Lige Technologies, Ag, Switzerland). DCM was obtained from Merck (Germany). Milli-Q water was supplied by a Milli-Q Plus System (Millipore Corporation, Bedford, USA). MCF-7 breast cancer cells and NIH/3T3 fibroblast cells were provided by American Type Culture Collection.

Preparation of Nanoparticles: The CPL NPs were prepared through a modified solvent extraction/evaporation single-emulsion method. A DCM solution (4 mL) containing 0.5 mg of CP and 50 mg of PLGA was poured into 60 mL of aqueous solution containing 0.5% (w/v) PVA as the emulsifier. This was followed by sonicating the mixture for 120 s at 18 W output using a microtip probe sonicator (XL2000, Misonix Incorporated, NY). The emulsion was then stirred at room temperature overnight to evaporate the DCM. The formed NP suspension was washed and centrifuged with MilliQ water three times to remove the excess emulsifier and free CP molecules. The obtained NP suspension was frozen and freeze-dried for two days to get the fine powder of NPs. To prepare pure PFV NPs without the PLGA matrix, a DCM solution (1 mL) containing 0.5 mg of PFV was poured into 60 mL of PVA aqueous solution, following the same procedure as that for the preparation of CPL NPs.

Characterization: The fluorescence spectra of the CPL NP aqueous suspensions were measured using a fluorometer (LS-55, Perkin Elmer, USA) with an excitation wavelength of 370, 407, 458, and 488 nm for the PF-, PFV-, PFBT-, and MEH-PPV-loaded NPs, respectively. The photograph of the CPL NP aqueous suspensions was taken using a digital color camera (EOS 400D, Canon, Japan) under a hand-held UV lamp with $\lambda_{\text{max}} = 365$ nm. Average particle size and size distribution of the CPL NPs were determined by LLS with a particle size analyzer (90 Plus, Brookhaven Instruments Co. USA) at a fixed angle of 90° at room temperature. The zeta potential of the CPL NPs was measured using a zeta potential analyzer (ZetaPlus, Brookhaven Instruments Corporation) at room temperature. The surface morphology of CPL NPs was investigated by FESEM (JSM-6700F, JEOL, Japan) at an accelerating voltage of 10 kV. The NPs were fixed on a stub with a double-sided sticky tape and then coated with a platinum layer using an autofine coater (JEOL, Tokyo, Japan) for 60 s in a vacuum at a current intensity of 10 mA. The morphology of CPL NPs was also studied by TEM (JEM-2010F, JEOL, Japan). The surface chemistry of PFV-loaded NPs and FA PFV-loaded NPs was studied by XPS (AXIS His-165 Ultra, Kratos Analytical, Shimadzu Corporation, Japan). The fixed transmission mode was utilized with a pass energy of 80 eV, and the binding energy spectrum was recorded from 0 to 1100 eV.

CP Encapsulation Efficiency: The CP encapsulation efficiency is defined as the ratio of the amount of CP successfully encapsulated in CPL NPs to the total amount of CP used in the fabrication of NPs. The fluorescence intensity of a series of DCM solutions (1 mL) with a designated CP concentration was analyzed using a fluorometer (LS-55, Perkin Elmer, USA) upon excitation at the absorption maximum for each CP. The standard curve of fluorescence intensity of CP versus its concentration was then constructed. A certain amount (0.5 mg) of freeze-dried CPL NPs powder was then dissolved in 1 mL of DCM, and the fluorescence intensity at the maximum emission was obtained using the fluorometer upon excitation at the absorption maximum for each CP. The amount of CP encapsulated in 0.5 mg of CPL NPs can be determined from the standard curve, and the encapsulation efficiency was calculated.

In vitro CP Release from CPL NPs: To determine the stability of the CPL NPs, 1 mg of NPs were suspended in 1 mL of $1 \times$ PBS buffer (PH 7.4) in a centrifuge tube and shook at 37°C in an orbital water bath shaker. At designated time intervals, the samples were centrifuged at 10 500 rpm for 15 min. The supernatant of the samples was individually extracted with 1 mL of DCM, and the fluorescence intensity of the DCM solution was monitored using a fluorometer (LS-55, Perkin Elmer, USA) upon excitation at the absorption maximum for each CP. The NPs were resuspended in $1 \times$ PBS buffer and put back in the orbital water bath for continuous study. The percentage of released CP molecules was expressed as the following equation:

$$\text{Released CP (\%)} = \frac{Int_{\text{sample}}}{Int_{\text{NP}}} \times 100\% \quad (1)$$

where Int_{sample} is the fluorescence intensity of the sample and Int_{NP} is the fluorescence intensity of the CP prepared by dissolving 1 mg of dried CPL NP powder in 1 mL of DCM solution.

Folate-Functionalization of PFV-Loaded NPs: Firstly, the amination of folic acid was carried out according to literature [22]. In brief, folic acid (441.4 mg, 1 mmol) was reacted with DCC (247.6 mg, 1.2 mmol) and NHS (230.18 mg, 2 mmol) in 30 mL of dimethylsulfoxide (DMSO) for 6 h at 50°C . The activated folic acid was then reacted with ethylene diamine (10 mmol) and pyridine (10 μg) at room temperature overnight. *N, N'*-dicyclohexylurea (DCU) was removed by filtration, and the crude product was then precipitated by addition of excess acetonitrile, filtered, and washed three times with diethyl ether. The aminated folic acid was collected after drying in a vacuum oven. The FA PFV-loaded PLGA NPs was then prepared as follows: PFV-loaded NPs (10 mg) were dispersed in 5 mL of Milli-Q water. After addition of EDAC (0.32 mg) and Sulfo-NHS (0.36 mg), the PFV-loaded PLGA NPs were activated for 2.5 h at room temperature. Borate buffer (5 mL, 0.2 M, pH = 8.5) was then added to the suspension, which was followed by the addition of 0.1 mL of aminated folic acid (0.1 M) in DMSO solution. The mixture was stirred at room temperature for 4 h and then washed and centrifuged with DMSO and water to eliminate the excess aminated folic acid. The FA PFV-loaded NPs were then collected for further study. Under the similar conditions, PFV-loaded NPs and aminated folic acid were mixed and stirred in the absence of EDAC and Sulfo-NHS. The obtained NPs were used as a control in the study of targeted cancer cell imaging.

Cell Cultures: MCF-7 breast cancer cells and NIH/3T3 fibroblast cells were cultured in folate-free RPMI 1640 medium containing 10% fetal bovine serum and 1% penicillin–streptomycin at 37°C in a humidified environment containing 5% CO_2 . Before experiment, the cells were precultured until confluence was reached.

Cell Imaging: MCF-7 cells were cultured in chamber (LAB-TEK, Chambered Coverglass System) at 37°C . After 80% confluence, the medium was removed, and the adherent cells were washed twice with $1 \times$ PBS buffer. The PFV-loaded NPs, FA PFV-loaded NPs or pure PFV NPs in RPMI 1640 medium at 87.5 nM PFV was then added to the chamber. After incubation for 2.5 h, cells were washed three times with $1 \times$ PBS buffer and then fixed by 75% ethanol for 20 min, which was further washed twice with $1 \times$ PBS buffer. The nuclei were stained with propidium iodide (PI) for 40 min. The cell monolayer was washed twice with $1 \times$ PBS buffer and imaged by CLSM (Zeiss LSM 410, Jena, Germany) with imaging software (Fluoview FV1000). The confocal images of NIH/3T3 cells treated with PFV-loaded NPs or FA PFV-loaded NPs under the same conditions were also studied. The CLSM images of MCF-7 cancer cells were also obtained after treatment with the other three types of CPL NPs at 87.5 nM CP under the same conditions.

Cellular Uptake: MCF-7 cells were seeded into 96-well black plates (Costar, IL, USA) for quantitative study of cellular uptake. After the cells reached 80% confluence, the medium was replaced with the suspension of PFV-loaded NPs, FA PFV-loaded NPs or pure PFV NPs in 100 μL of folate-free RPMI 1640 medium at 87.5 nM PFV. The cells were then cultured at 37°C for 2.5 h. For each sample, six wells were used for positive control without adding NP suspensions and another six wells were used for NP samples. After incubation for 2.5 h, the sample wells were washed three times with 50 μL $1 \times$ PBS buffer to remove traces of NPs. Folate-free RPMI 1640 medium (100 μL) was then added to each sample well, which was followed by the addition of 50 μL of 0.5% Triton X-100 in 0.2 N NaOH to both positive control and sample wells to lyse the cells. The fluorescence intensity of NPs present in each well was then measured by the microplate reader (Genios Tecan) with excitation wavelength of 407 nm. The fluorescence intensity was collected at 481 nm. The cellular uptake efficiency was expressed as the ratio of the fluorescence in the sample wells to that of the positive control.

Cytotoxicity of CPL NPs: MTT assays were performed to assess the metabolic activity of NIH/3T3 fibroblast cells. NIH/3T3 cells were seeded in 96-well plates (Costar, IL, USA) at an intensity of 4×10^4 cells mL^{-1} . After 24 h incubation, the medium was replaced by the PFV-loaded NP or pure PFV NP suspension at PFV concentrations of 87.5, 350, and 700 nM, and the cells were then incubated for 12, 24, and 48 h, respectively. After the designated time intervals, the wells were washed twice with $1 \times$ PBS buffer, and 100 μL of freshly prepared MTT (0.5 mg mL^{-1}) solution in culture medium was added to each well. The MTT medium solution was carefully

removed after 3 h incubation in the incubator. Isopropanol (100 μ L) was then added into each well, and the plate was gently shaken for 10 min at room temperature to dissolve all precipitates formed. The absorbance of MTT at 570 nm was monitored by the microplate reader (Genios Tecan). Cell viability was expressed by the ratio of absorbance of the cells incubated with NP suspension to that of the cells incubated with culture medium only. To evaluate the cytotoxicity of the other three types of CPL NPs, NIH/3T3 cells were incubated with CPL NP suspension at CP concentrations of 87.5, 350, and 700 nm for 48 h, individually. The metabolic viability of NIH/3T3 cells was then evaluated, following the same procedure as that in the evaluation of the cytotoxicity of PFV-loaded NPs.

Acknowledgements

The authors are grateful to the National University of Singapore (R-279-000-234-123) and Singapore Ministry of Education (R-279-000-255-112) for financial support. The authors also thank Zhang Jie and Hu Xian for technical support in confocal laser scanning microscopy (CLSM) imaging experiments. K. Li thanks NUS for support via a research fellowship. Supporting Information is available online from Wiley InterScience or from the author.

Received: June 22, 2009

Published online: October 19, 2009

- [1] a) A. P. Alivisatos, *Science* **1996**, 271, 933. b) M. Ferrari, *Nat. Rev. Cancer* **2005**, 5, 161.
- [2] J. Zhang, R. E. Campbell, A. Y. Ting, R. T. Tsien, *Nat. Rev. Mol. Cell Biol.* **2002**, 3, 906.
- [3] A. M. Koch, F. Reynolds, M. F. Kircher, H. P. Merkle, R. Weissleder, L. Josephson, *Bioconjugate Chem.* **2003**, 14, 1115.
- [4] a) A. P. Alivisatos, *Nat. Biotechnol.* **2004**, 22, 47. b) M. E. Akerman, W. C. W. Chan, P. Laakkonen, S. N. Bhatia, E. Ruoslahti, *Proc. Natl. Acad. Sci. USA* **2002**, 99, 12617. c) C. M. Niemeyer, *Angew. Chem. Int. Ed.* **2001**, 40, 4128.
- [5] a) X. H. Gao, Y. Cui, R. M. Levenson, L. W. K. Chung, S. Nie, *Nat. Biotechnol.* **2004**, 22, 969. b) W. C. W. Chan, S. M. Nie, *Science* **1998**, 281, 2016. c) M. V. Yezhelyev, A. Al-Hajj, C. Morris, A. I. Marcus, T. Liu, M. Lewis, C. Cohen, P. Zrazhevskiy, J. W. Simons, A. Rogatko, S. Nie, X. Gao, R. M. O'Regan, *Adv. Mater.* **2007**, 19, 3146.
- [6] X. Michalet, F. F. Pinaud, L. A. Bentolila, J. M. Tsay, S. Doose, J. J. Li, G. Sundaresan, A. M. Wu, S. S. Gambhir, S. Weiss, *Science* **2005**, 307, 538.
- [7] a) B. Dubertret, P. Skourides, D. J. Norris, V. Noireaux, A. H. Brivanlou, A. Alibchaber, *Science* **2002**, 298, 1759. b) A. M. Derfus, W. C. W. Chan, S. N. Bhatia, *Nano Lett.* **2004**, 4, 11. c) A. M. Smith, H. Duan, A. M. Mohs, S. Nie, *Adv. Drug Delivery Rev.* **2008**, 60, 1226.
- [8] D. T. McQuade, A. E. Pullen, T. M. Swager, *Chem. Rev.* **2000**, 100, 2537.
- [9] a) R. H. Friend, R. W. Gymer, A. B. Holmes, J. H. Burroughes, R. N. Marks, C. Taliani, D. D. C. Bradley, D. A. Dos Santos, J.-L. Brédas, M. Logdlund, W. R. Salaneck, *Nature* **1999**, 397, 121. b) G. Gustafsson, Y. Cao, G. M. Treacy, F. Klavetter, N. Colaneri, A. J. Heeger, *Nature* **1992**, 357, 477. c) J. J. M. Halls, C. A. Walsh, N. C. Greenham, E. A. Marseglia, R. H. Friend, S. C. Moratti, A. B. Holmes, *Nature* **1995**, 376, 498. d) S. W. Thomas, III, G. D. Joly, T. M. Swager, *Chem. Rev.* **2007**, 107, 1339.
- [10] a) J. H. Moon, W. McDaniel, P. MacLean, L. F. Hancock, *Angew. Chem. Int. Ed.* **2007**, 46, 8223. b) I. Kim, H. Shin, A. J. Garcia, U. H. F. Bunz, *Bioconjugate Chem.* **2007**, 18, 815. c) R. L. McRae, R. L. Phillips, I. Kim, U. H. F. Bunz, C. J. Fahrni, *J. Am. Chem. Soc.* **2008**, 130, 8844.
- [11] a) C. Szymanski, C. F. Wu, J. Hooper, M. A. Salazar, A. Perdomo, A. Dukes, J. McNeill, *J. Phys. Chem. B* **2005**, 109, 8543. b) C. F. Wu, B. Bull, C. Szymanski, K. Christensen, J. McNeill, *ACS Nano* **2008**, 2, 2415.
- [12] Y. W. Khin, S. S. Feng, *Biomaterials* **2005**, 26, 2713.
- [13] G. Padmanaban, S. Ramakrishnan, *J. Phys. Chem. B* **2004**, 108, 14933.
- [14] C. F. Wu, H. Peng, Y. Jiang, J. McNeill, *J. Phys. Chem. B* **2006**, 110, 14148.
- [15] K. A. Foster, M. Yazdaniyan, K. L. Audus, *J. Pharm. Pharmacol.* **2001**, 53, 57.
- [16] M. G. Qaddoumi, H. Ueda, J. Yang, J. Davda, V. Labhasetwar, V. H. L. Lee, *Pharm. Res.* **2004**, 21, 641.
- [17] H. J. Dou, M. Jiang, H. S. Peng, D. Y. Chen, Y. Hong, *Angew. Chem. Int. Ed.* **2003**, 42, 1516.
- [18] M. A. Dobrovolskaia, S. E. McNeil, *Nat. Nanotechnol.* **2007**, 2, 469.
- [19] Y. J. Lu, P. S. Low, *J. Controlled Release* **2003**, 91, 17.
- [20] a) C. P. Leamon, J. A. Reddy, *Adv. Drug Delivery Rev.* **2004**, 56, 1127. b) Y. J. Lu, E. Segal, C. P. Leamon, P. S. Low, *Adv. Drug Delivery Rev.* **2004**, 56, 1161.
- [21] a) V. Dixit, J. V. Bossche, D. M. Sherman, D. H. Thompson, R. P. Andres, *Bioconjugate Chem.* **2006**, 17, 603. b) J. Sudimack, R. J. Lee, *Adv. Drug Delivery Rev.* **2000**, 41, 147.
- [22] E. S. Lee, K. Na, Y. H. Bae, *J. Controlled Release* **2003**, 91, 103.
- [23] a) K. Y. Pu, Z. Fang, B. Liu, *Adv. Funct. Mater.* **2008**, 18, 1321. b) K. Y. Pu, B. Liu, *Adv. Funct. Mater.* **2009**, 19, 277.